A Detailed Map of the 660-Kilometer Discontinuity Beneath the Izu-Bonin Subduction Zone

Charles W. Wicks, Jr.,* and Mark A. Richards

Dynamical processes in the Earth's mantle, such as cold downwelling at subduction zones, cause deformations of the solid-state phase change that produces a seismic discontinuity near a depth of 660 kilometers. Observations of short-period, shear-to-compressional wave conversions produced at the discontinuity yield a detailed map of deformation beneath the Izu-Bonin subduction zone. The discontinuity is depressed by about 60 kilometers beneath the coldest part of the subducted slab, with a deformation profile consistent with the expected thermal signature of the slab, the experimentally determined Clapeyron slope of the phase transition, and the regional tectonic history.

The 660 discontinuity, which is commonly regarded as the boundary between the upper and lower mantle of the Earth, is characterized by a ~5 to 10% increase with depth in seismic velocities and density (*1*). It is uncertain whether the discontinuity is coincident with a chemical boundary between two isolated, or nearly isolated, mantle reservoirs. However, the existence of a solid-solid phase change (from upper mantle minerals dominated by γ spinel to an assemblage of lower mantle minerals dominated by silicate-perovskite) near a depth of 660 km has been known for some time (*2*).

The 660 discontinuity is also known to be sharp (~5 km in width) from observations that short-period waves both convert at and reflect off of the interface. The sharpness of the discontinuity has led to speculation that it may also represent a change in bulk chemistry (*3, 4*). High-pressure experiments and seismic observations have led to a consensus that the sharpness of the 660 discontinuity results from the phase change of γ spinel to perovskite. This phase change occurs within a small depth interval (~5 km) (*5, 6*) with a small negative Clapeyron slope [~−2.8 MPa K^{-1} for the transition from γ spinel to silicate-perovskite plus magnesiowüstite (*5*)]. The transition occurs at a depth near 660 km, nearly independent of the bulk chemistries expected in the mantle (*5, 7*). Cold temperatures in a subducted slab should depress this phase change up to ~60 km. By contrast, the dynamical depression of a chemical boundary beneath subduction zones should reach a minimum of ~100 to 300 km. To date, seismic studies have found a maximum of only ~30 km of depth variation of the 660 discontinuity (*8–13*), consistent with a solid-state phase change with a small negative Clapeyron slope. To constrain further the dynamical significance of the 660 discontinuity, high-resolution seismic images of topography on the discontinuity are needed. In this report, we present a detailed map of the 660 topography beneath the Izu-Bonin subduction zone.

We measured topography on the 660 discontinuity beneath the Izu-Bonin trench using short-period (~1-Hz) observations of the seismic phase $S_{660}P$, which starts as a downgoing S wave that partially converts to a downgoing P wave at the 660 discontinuity beneath the source. The length of the slower S leg of the path is proportional to the time interval between the $S_{660}P$ and P arrivals. We used the difference in the travel times of the two phases, $S_{660}P - P$, to determine the apparent conversion depth in an IASP91 velocity model (*1*) that was modified to include a 660 discontinuity that varies in depth. The apparent conversion depth of $S_{660}P$ is then used to infer the depth of the 660 discontinuity. The sources are deep earthquakes in the Izu-Bonin subduction zone and the receiver is the Warramunga seismic array (WRA) in north-central Australia (Fig. 1).

The phase $S_{660}P$ is akin to the depth phase pP (*14*) in that the time delays of $S_{660}P - P$ and $pP - P$ are each fairly insensitive to epicentral location but are very sensitive to hypocentral depth. For example, for a typical Izu-Bonin event located at an epicentral distance from the WRA of 5300 km and a depth of 400 km, a difference in epicentral distance of 50 km translates to less than 0.2 s of difference in the time delay $pP - P$ and less than 0.1 s difference in $S_{660}P - P$. In contrast, a difference in hypocentral depth of 50 km translates to over 7 s of difference in $pP - P$ and over 5 s difference in $S_{660}P - P$. Also for this event, a shift of 50 km in the depth of the 660 discontinuity equates to nearly 5 s of difference in $S_{660}P - P$ time delay. Therefore, accurate estimates of the local depression of the 660 discontinuity are possible only if we obtain accurate estimates of the hypocentral depths for the 73 deep (>250-km hypocentral depth) earthquakes used in our study. We obtained accurate estimates of the earthquake hypocenters by using the time interval $pP - P$ or $pwP - P$ (*15*).

The phase $S_{660}P$ can be reliably identified in short-period array recordings (*8–10*) and can be consistently observed where source radiation patterns are favorable (*16*). For the Izu-Bonin events we used, favorable radiation patterns and source-receiver geometry result in many high-amplitude $S_{660}P$ phases (Fig. 2). For each of the earthquakes, we processed the 20 vertical channels of the WRA using a nonlinear stacking technique

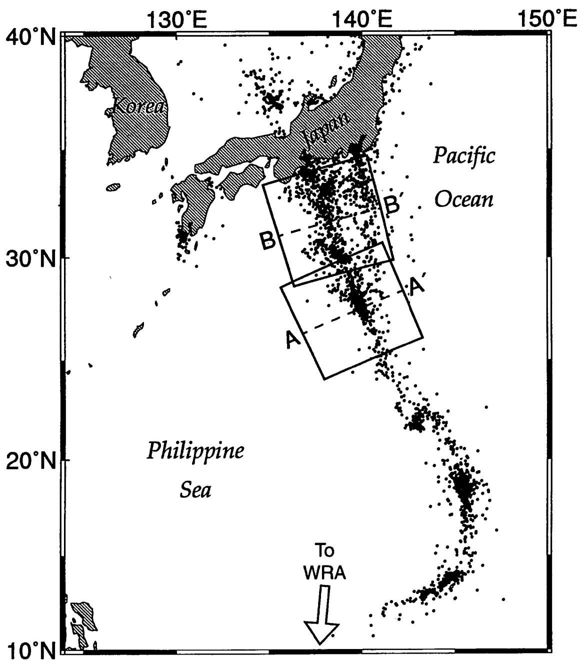

Fig. 1. A map of the study area. Detailed study windows A and B are drawn around events with neighboring pP bounce points, events that also have neighboring $S_{660}P$ conversion points. International Seismology Center (ISC) earthquake locations deeper than 100 km are labeled with small solid dots to show the location of the Izu-Bonin and Marianas deep Wadati-Benioff zones. The WRA is ~5000 km south of the study area.

C. W. Wicks, Jr., Department of Geology and Geophysics, University of California at Berkeley, Berkeley, CA 94720.
M. A. Richards, Geophysics Program, AK-50, University of Washington, Seattle, WA 98195.
*To whom correspondence should be addressed.

(*10*) that resulted in a rectified seismogram (Fig. 2). This processing brings out phases with similar apparent wavefront velocity across the WRA, such as *P*, $S_{660}P$, *pP*, and *pwP* (*14*). From the original 73 events, we selected 42 events to use. We selected only the events that displayed both prominent $S_{660}P$ and *pwP* phases to ensure good depth estimates of the 660 discontinuity.

As shown in Fig. 3, the 660 discontinuity is depressed ~40 km in window A. The full extent of the anomaly along A-A′ may not have been measured and only one poorly constrained data point limits it on the west, but the depression appears to be ~200 to 300 km wide. This broad anomaly agrees with the slab thickening of two to three times predicted by the numerical modeling of a steeply dipping slab encountering a viscosity contrast (*17*). The anomaly also agrees with slab thickening near the 660 discontinuity presented as a possible model by residual sphere analysis in the Tonga subduction zone (*18, 19*).

A comparison of the apparent depth of the 660 discontinuity in window A from three different hypocenter data sets (Fig. 4) shows that the magnitude of the depth anomaly does not change significantly among the three determinations. The apparent deflection of the discontinuity does shift ~10 km deeper from Fig. 4A to Fig. 4, B and C, and the anomaly appears broadest in Fig. 4C. The points between 2° and 3° (Fig. 4) sample the maximum depression of the discontinuity and probably sample the 660 discontinuity within the cold core of the subducted Izu-Bonin slab.

To test the sensitivity of our results to near source velocity anomalies, we estimated the bounds on 660 topography by redetermining hypocentral depths for the events (using observed $pwP - P$ or $pP - P$ time intervals) and redetermining the depth of the 660 discontinuity (using observed $S_{660}P - P$ time intervals) for slab models that were both faster and slower than the IASP91 reference model (*20*). We used the redetermined values for the depth of the 660 discontinuity for these two velocity models combined with estimated reading errors for the phases for each event to calculate the error bars (*21*) assigned to the depth determinations (Fig. 4C). In window B (Fig. 5), the 660 discontinuity is depressed more than 50 km in an anomaly that appears open-ended to the west and abruptly limited to the east. The size of the anomaly is fairly robust in that the local depression of the 660 discontinuity is ~60 km for each hypocenter data set.

The deflections of the 660 discontinuity that we determined in windows A and B are larger than those found by others (*8–13*), probably because we are probing a colder and more confined thermal anomaly than has been studied before (*22*). Our error estimates suggest a deflection of between 46 and 80 km in the coldest part of the slab, which we take to be 1000 ± 200 K colder than the ambient mantle. This temperature results in an estimated Clapeyron slope for the phase boundary from γ spinel to perovskite of −1.7 to −4.4 MPa K^{-1} (*23*). This estimate compares well with the value of −2.8 MPa K^{-1} in (*5*) and is lower than −4.0 ± 2.0 MPa K^{-1} found in (*24*). More importantly, the range of values has an estimated error of ±1.35 MPa K^{-1}, less than that of ±2.0 MPa K^{-1} in (*24*). With a better thermal model of the slab and the incorporation of $S_{660}P$ times into a tomography model, we should be able to offer a more accurate determination of the Clapeyron slope.

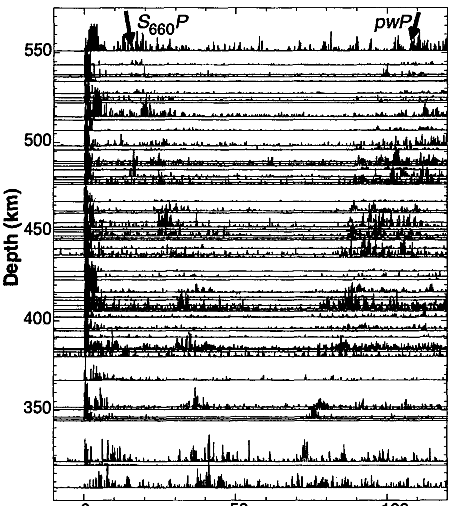

Fig. 2. Section of the hypocentral depth record of the events used in this study. Each trace is a processed WRA seismogram for a single event, plotted at the hypocentral depth found by Engdahl and colleagues (*25, 28*). Phases $S_{660}P$ and *pwP* are prominent along the directions of the labeled arrows. Time is relative to the onset of *P*. Although the seismograms are from earthquakes that span over 1000 km of epicentral distance, the robust sensitivity of $S_{660}P - P$ and $pwP - P$ on depth and their insensitivity to distance are apparent.

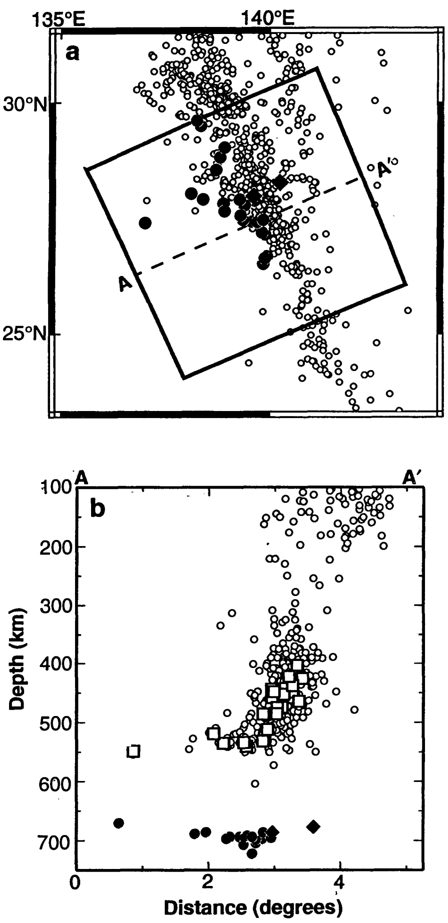

Fig. 3. Details for window A. The ISC earthquake locations are shown as hollow circles, the conversion points for $S_{660}P$ found in this study are shown as solid circles, and the conversion points for $S_{660}P$ from the study by Vidale and Benz (*13*) are shown as solid diamonds. (**a**) Location map for window A. (**b**) Projection of hypocenters and $S_{660}P$ conversion points on a vertical plane through A–A′, perpendicular to the strike of the deep Wadati-Benioff zone. The hollow squares represent Engdahl and co-workers' hypocenters (*25, 28*) for events that also have an $S_{660}P$ conversion point.

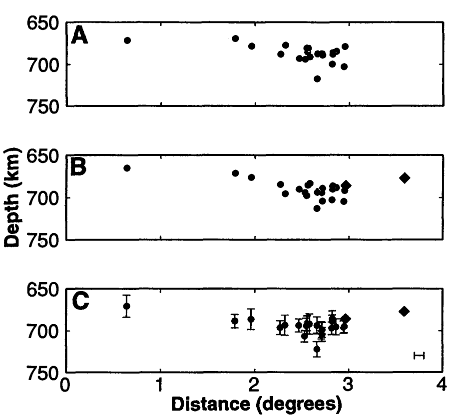

Fig. 4. Projection of $S_{660}P$ conversion points from window A on a small area of cross section A–A′ for three different hypocenter data sets. The solid circles represent $S_{660}P$ conversion points determined in this study, and the solid diamonds represent $S_{660}P$ conversion points of Vidale and Benz (*13*). (**A**) Hypocenters from the ISC catalog (*43*) located in the reference velocity model of Jeffreys and Bullen (*44*). (**B**) Hypocenters provided by Engdahl and co-workers (*25, 28*), who utilized *pP* and water depth to locate the events using the IASP91 reference model. (**C**) Hypocenters found with the use of *pwP* in this study. The horizontal error bar in the lower right corner represents the worst standard error in the location of the earthquakes we used, as reported in the ISC catalog. This error bar should represent a good estimate of the horizontal error of the conversion point locations.

Tomographic images of the Izu-Bonin subduction zone (*25, 26*) have been interpreted to suggest that the subducted Izu-Bonin slab lies horizontally atop the 660 discontinuity beneath the Philippine plate. Although the horizontal lying slab has been described as being deflected by the 660 discontinuity, the slab may have been deposited on the discontinuity during an episode of eastward trench retreat (*25, 27*) at a time of back-arc spreading. Such an episode may also be largely responsible for the presence of other apparently horizontally lying slab structures beneath the Kurile and Japan subduction zones (*26*) that, like the Izu-Bonin subduction zone, underlie back-arc basins (*29*).

The Izu-Bonin trench retreated eastward from about 25 million to 15 million years ago during the opening of the Shikoku basin in the East Philippine Sea (*30*). The northern Izu-Bonin subduction zone has been stationary in the hot-spot reference frame for the last 15 million years, whereas the southern part has experienced westward trench advance for the last 5 million years (*31*). Thus, trench advance may explain the interpreted broad thermal depression found in window A (Figs. 3 and 4). By contrast, the abrupt increase in depression of the 660 discontinuity on the east side of the Wadati-Benioff zone found in window B (Fig. 5) may result from a lack of trench advance in the northern end of the Izu-Bonin subduction zone.

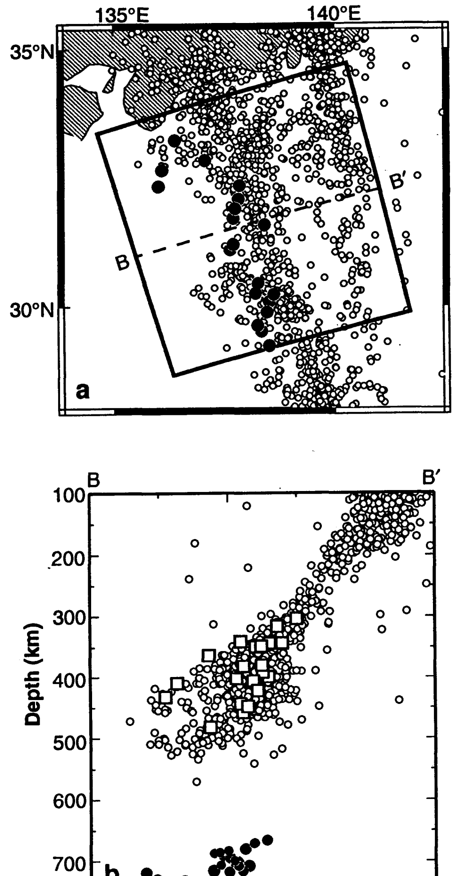

Fig. 5. Details for window B, similar to Fig. 3. (**a**) Location map for window B. (**b**) Projection of hypocenters and $S_{660}P$ conversion points on a vertical plane through cross section B–B′, perpendicular to the strike of the deep Wadati-Benioff zone. We determined the hypocenters using $pP - P$ or $pwP - P$ and estimated the errors using the same method as described for Fig. 4C. The size of each solid circle in this projection is scaled to the estimated error of the depth to the 660 discontinuity for each $S_{660}P$ conversion point. The symbols are the same as in Fig. 3.

The fate of the slab below the 660 discontinuity is unknown. There remains some evidence that the lower mantle and upper mantle are chemically distinct (*32–34*), and slab penetration of the 660 discontinuity does not necessarily require a homogeneous mantle. However, seismic tomography indicates that in some cases slabs do penetrate deep into the lower mantle (*26*). With modest assumptions of threefold thickening of the slab below a depth of 660 km and a subduction rate of 6 cm $year^{-1}$, the regional plate tectonic history suggests that the Izu-Bonin slab could extend ~300 km into the lower mantle. Such an extension is not observed in tomographic studies of the area (*25, 26*), but there is reason to believe that once the slab passes through the 660 discontinuity its material properties would make it nearly invisible to seismic body waves (*7, 35*). However, if slabs are invisible below the 660 discontinuity, what is the nature of high-velocity extensions of slabs to depths of ~1200 km, such as seen in the Java subduction zone (*26*)?

As pointed out by Wahr and colleagues (*36*), topography on the 660 discontinuity may have unmodeled effects on seismic velocity inversions, particularly in subduction zones. The area of 660 depression will cause a pronounced low-velocity anomaly. A high-frequency *P* wave that samples 60 km of depression in the 660 discontinuity (~7% slow) could sample nearly 200 km of slab material in the lower mantle that is 2% faster than the surrounding mantle with no net travel-time anomaly. This type of compensation could be a problem in tomographic studies of areas with short extensions of the slab into the lower mantle. A short slab extension is expected from plate reconstructions in the Izu-Bonin subduction zone, but longer extensions into the lower mantle may be expected elsewhere, such as observed in the Java subduction zone (*26*).

REFERENCES AND NOTES

1. B. L. N. Kennet and E. R. Engdahl, *Geophys. J. Int.* **105**, 429 (1991).
2. L. G. Liu, *Nature* **262**, 770 (1976).
3. R. Jeanloz and A. B. Thompson, *Rev. Geophys. Space Phys.* **21**, 51 (1983).
4. A. C. Lees, M. S. T. Bukowinski, R. Jeanloz, *J. Geophys. Res.* **88**, 8145 (1983).
5. E. Ito and E. Takahashi, *ibid.* **94**, 10637 (1989).
6. R. Boehler and A. Chopelas, *Geophys. Res. Lett.* **18**, 1147 (1991).
7. R. Jeanloz, *ibid.*, p. 1743.
8. B. J. Barley, J. A. Hudson, A. Douglas, *Geophys. J. R. Astron. Soc.* **69**, 159 (1982).
9. G. Bock and J. Ha, *ibid.* **77**, 593 (1984).
10. M. A. Richards and C. W. Wicks, Jr., *Geophys. J. Int.* **101**, 1 (1990).
11. J. Revenaugh and T. H. Jordan, *J. Geophys. Res.* **96**, 19763 (1991).
12. P. M. Shearer and T. G. Masters, *Nature* **355**, 791 (1992).
13. J. E. Vidale and H. M. Benz, *ibid.* **356**, 678 (1992).
14. The depth phase *pP* leaves the source as an upgoing *P* wave that subsequently reflects from the rock-sediment interface, whereas *pwP* is the reflection at the water-air interface. Generally, in short-period studies such as ours *pwP* is observed although *pP* does not always precede it. The *pP depth phase is probably not observed where the rock-sediment interface is too diffuse to reflect short-period energy.*
15. We use Engdahl and colleagues' epicentral location (*25, 28*) and the time interval $pP - P$ or $pwP - P$ to find the hypocentral depth in an IASP91 Earth model that has been modified to include a water layer and sediment layer appropriate for a given *pP* reflection point. Because $pP - P$ is more robust to errors in ocean depth than $pwP - P$, preference was given to $pP - P$ when both *pP* and *pwP* were present.
16. C. W. Wicks, Jr., and M. A. Richards, *Geophys. J. Int.* **107**, 279 (1991).
17. M. Gurnis and B. H. Hager, *Nature* **335**, 317 (1988).
18. K. M. Fischer, T. H. Jordan, K. C. Creager, *J. Geophys. Res.* **93**, 4773 (1988).
19. K. M. Fischer, thesis, Massachusetts Institute of Technology (1988).
20. We base a fast slab model on tomographic studies that indicate that the Izu-Bonin slab is ~3% faster than the IASP91 model (*25, 26*). Our slab model is 3% faster than the IASP91 model from depths of 200 to 660 km. For a slow slab model, we choose a slab that is 3% faster than the IASPI91 model from depths of 200 to 410 km and 3% slower than IASP91 from depths of 410 to 660 km. The existence of a metastable wedge of slow material has been theorized as a source for deep earthquakes (*37, 38*), and there is some observational evidence suggesting its presence in the Izu-Bonin slab (*39, 40*). The slow slab assumption seems to contradict the results of tomography studies, but tomography involves the smoothing of velocity perturbations, especially such small-scale perturbations as can be expected for a metastable wedge. The assumption that the whole slab is slow between depths of 410 and 660 km is a generous extreme bound.
21. The errors in the choice of arrival times were generally small, from ±0.1 to ±0.3 s, but were as large as ±0.9 s for a single phase. An error of 0.1 s in the choice of any one phase results in an uncertainty in the depth of the 660 discontinuity of ~1 km. Unmodeled errors are possible from velocity heterogeneities above a 200-km depth, inaccurate water depth at the *pP* bounce point, a choice of the wrong phase, and the choice of $S_{660}P$ on emergent phases, such as in the case for the deepest conversion point shown in Figs. 3 and 4. In addition, some of the $S_{660}P$ phases were multiple in nature, in which case we picked the first arriving pulse. The multiple nature of some $S_{660}P$ phases still requires characterization, but we think the most likely explanation is near-source heterogeneity effects.
22. In our previous study using $S_{660}P$ in the Tonga subduction zone (*10*), we found ~30 km of deflection. With the use of better hypocenter locations (*25, 28*) and of individual events to look at the depression of the 660 discontinuity, we may

be able to refine our previous results.
23. To make this estimate, we assume that only the phase-change boundary from γ spinel to perovskite is responsible for $S_{660}P$. We also assume that the shallowest $S_{660}P$ depth represents wave conversion in the ambient mantle. The temperature estimated for the coldest part of the Izu-Bonin slab is 900 ± 100 K (*41*), whereas the mantle temperature of the phase change from γ spinel to silicate-perovskite and magnesiowüstite near a depth of 660 km is 1900 ± 100 K (*6*).
24. E. Ito, M. Akaogi, L. Topor, A. Navrotsky, *Science* **249**, 1275 (1990).
25. R. van der Hilst, R. Engdahl, W. Spakman, G. Nolet, *Nature* **353**, 37 (1991).
26. Y. Fukao, M. Obayashi, H. Inoue, M. Nenbai, *J. Geophys. Res.* **97**, 4809 (1992).
27. Trench advance or trench retreat is relative to an immobile, or slowly moving, lower mantle.
28. R. D. van der Hilst and E. R. Engdahl, *Geophys. J. Int.* **106**, 169 (1991).
29. C. Park, K. Tamaki, K. Kobayashi, *Tectonophysics* **181**, 351 (1990).
30. T. Seno and S. Maruyama, *ibid.* **102**, 53 (1984).
31. Trench-advance rates over the last 5 million years increased linearly from 0 to 6 mm year^{-1} near Japan to 24 to 30 mm year^{-1} at a latitude of 27°N (*42*). Westward trench advance appears to have steepened the slab dip (*42*), which is roughly 50° near Japan and 80° near 27°N. The southern Izu-Bonin trench has only advanced toward Eurasia a maximum of 150 km in the last 5 million years, and the northern part has remained nearly fixed.
32. R. Jeanloz and E. Knittle, *Philos. Trans. R. Soc. London Ser. A* **328**, 377 (1989).
33. M. S. T. Bukowinski and G. H. Wolf, *J. Geophys. Res.* **95**, 12583 (1990).
34. L. Stixrude, R. J. Hemley, Y. Fei, H. K. Mao, *Science* **257**, 1099 (1992).
35. D. L. Anderson, *Theory of the Earth* (Blackwell, Boston, 1989).
36. J. Wahr, M. Ritzwoller, A. Rodgers, V. Dehant, *Eos* **73**, 518 (1992).
37. C. Sung and R. G. Burns, *Tectonophysics* **31**, 1 (1976).
38. S. H. Kirby, W. B. Durham, L. A. Stern, *Science* **252**, 216 (1991).
39. S. W. Roeker, *J. Geophys. Res.* **90**, 7771 (1985).
40. T. Iidaka and D. Suetsugu, *Nature* **356**, 593 (1992).
41. C. Meade and R. Jeanloz, *Science* **252**, 68 (1991).
42. R. L. Carlson and C. A. Mortera-Gutiérrez, *Tectonophysics* **181**, 331 (1990).
43. We use International Seismology Center (ISC) hypocenters that were determined from the direct *P* arrivals only. For some of the events the ISC catalog also contains hypocenters determined with *pP*, but for the sake of consistency, we use the hypocenters determined from *P*.
44. H. Jeffreys and K. E. Bullen, *Seismological Tables* (Smith and Ritchie, Edinburgh, 1970).
45. We thank E. R. Engdahl for access to his set of earthquake locations; R. Gritto and L. Stixrude for their helpful discussions; and J. Vidale, P. Shearer, and M. Bukowinski, whose comments helped improve the manuscript. Supported by National Science Foundation grant EAR9004026.

4 May 1993; accepted 29 July 1993

Comparisons Between Seismic Earth Structures and Mantle Flow Models Based on Radial Correlation Functions

Thomas H. Jordan, Peter Puster, Gary A. Glatzmaier, Paul J. Tackley

Three-dimensional numerical simulations were conducted of mantle convection in which flow through the transition zone is impeded by either a strong chemical change or an endothermic phase change. The temperature fields obtained from these models display a well-defined minimum in the vertical correlation length at or near the radius where the barrier is imposed, even when the fields were filtered to low angular and radial resolutions. However, evidence for such a feature is lacking in the shear-velocity models derived by seismic tomography. This comparison suggests that any stratification induced by phase or chemical changes across the mid-mantle transition zone has a relatively small effect on the large-scale circulation of mantle material.

One goal of structural seismology is to map variations in the seismic wave speeds in sufficient detail to resolve the pattern of the mantle convection. The most fundamental issue is the degree to which the large-scale flow is stratified by changes in mineralogical phase or bulk chemistry across the transition zone from depths of 400 to 700 km (*1*). Particular attention is being paid to the role of the 670-km discontinuity, which is dominated by the endothermic dissociation of spinel $(Mg,Fe)_2SiO_4$ into perovskite $(Mg,Fe)SiO_3$ plus $(Mg,Fe)O$. Laboratory (*2*) and seismic observations (*3*) constrain the Clapeyron slope of this phase transition to be negative and relatively steep: -4 ± 2 MPa K^{-1}. Convection calculations that combine phase-change dynamics with two-dimensional (2D) (*4, 5*) and 3D (*6, 7*) flow geometries indicate that an endothermic transition of this magnitude acts to inhibit convection through the phase boundary.

Any restriction of the large-scale flow by this or some other mechanism (*8*) should be evident in the shear-wave speeds determined by seismic tomography. Seismic data sets have been inverted by several research groups (*9–13*) to obtain the shear-velocity perturbation $\delta\beta(r,\Omega)$ up to spherical harmonic degree 12 throughout the mantle, where r is the radius ranging from the core-mantle boundary at $b = 3480$ km to the surface at $a = 6371$ km and $\Omega = (\theta,\varphi)$, a point on the geographic sphere S_1. In regions where compositional and phase differences can be ignored, $\delta\beta(r,\Omega)$ is relatively small, typically less than 5% of the mean wave speed, and can be related to the aspherical temperature variations by the linear approximation

$$\delta\beta(r,\Omega) = (\partial\beta/\partial T)_P \, \delta T(r,\Omega) \qquad (1)$$

Progress in the calculation of 3D, solid-state convection (*6, 7, 14, 15*) makes it feasible to discriminate among the various stratification hypotheses by the comparison of numerical simulations of δT with seismic estimates of $\delta\beta$ throughout the entire mantle.

A direct comparison of the temperature and shear-velocity fields is not the best approach, however. Convection models are still too crude to predict the details of mantle flow. Moreover, whole-mantle (WM) tomography cannot resolve such details, and there is still considerable uncertainty in the value of $(\partial\beta/\partial T)_P$ in the lower mantle (*16*). Competing convection hypotheses must therefore be tested by consideration of the average properties of the temperature field that can be reliably derived from low-resolution estimates of the seismic velocities and that are robust with respect to the δT-$\delta\beta$ scaling. In most tomographic inversions, the shear-speed variations are represented by a truncated series

$$\delta\beta(r,\Omega) = \sum_{l=1}^{l_{max}} \sum_{m=-l}^{l} \delta\beta_l^m(r) Y_l^m(\Omega) \qquad (2)$$

where $b \leq r \leq a$ and Y_l^m is the surface spherical harmonic of angular degree l and azimuthal order m. For hypotheses regarding convective stratification, the most obvious discriminants are radial functions constructed by some sort of averaging over the angular coordinates. An example is the angular squared-amplitude (power) spectrum, $S_\beta(r,l) = \sum_m |\delta\beta_l^m(r)|^2$. Tomographic estimates of $S_\beta(r,l)$ display high amplitudes and low characteristic wave numbers in both the uppermost and lowermost mantle (*9–12*). These estimates have been interpreted as manifestations of thermal, and perhaps chemical, boundary layers at the top and the bottom of the mantle (*9, 18*). The $S_\beta(r,l)$ spectrum peaks at $l = 4$ to 5 in

T. H. Jordan and P. Puster, Department of Earth, Atmospheric, and Planetary Sciences, Massachusetts Institute of Technology, Cambridge, MA 02139.
G. A. Glatzmaier, Earth and Environmental Science Division and Institute of Geophysics and Planetary Physics, Los Alamos National Laboratory, Los Alamos, NM 87545.
P. J. Tackley, Seismological Laboratory, California Institute of Technology, Pasadena, CA 91125.